

Out-of-distribution detection using normalizing flows on the data manifold

Seyedeh Fatemeh Razavi^a, Mohammad Mahdi Mehmanchi^a, Reshad Hosseini^{a,*}, Mostafa Tavassolipour^a

^a*School of ECE, College of Engineering, University of Tehran, Tehran, Iran*

Abstract

A common approach for out-of-distribution detection involves estimating an underlying data distribution, which assigns a lower likelihood value to out-of-distribution data. Normalizing flows are likelihood-based generative models providing a tractable density estimation via dimension-preserving invertible transformations. Conventional normalizing flows are prone to fail in out-of-distribution detection, because of the well-known curse of dimensionality problem of the likelihood-based models. According to the manifold hypothesis, real-world data often lie on a low-dimensional manifold. This study investigates the effect of manifold learning using normalizing flows on out-of-distribution detection. We proceed by estimating the density on a low-dimensional manifold, coupled with measuring the distance from the manifold, as criteria for out-of-distribution detection. However, individually, each of them is insufficient for this task. The extensive experimental results show that manifold learning improves the out-of-distribution detection ability of a class of likelihood-based models known as normalizing flows. This improvement is achieved without modifying the model structure or using auxiliary out-of-distribution data during training.

Keywords: Generative models, Manifold learning, Normalizing flows, Out-of-distribution

1. Introduction

Out-Of-Distribution (OOD) detection classifies test data into in-/out- of distribution data (Yang et al., 2022). Generative models that rely on the likelihood estimation are a prominent candidate for detecting OOD data. It is expected they can assign low likelihood value to OOD data. However, high-dimensional likelihood-based generative models are susceptible to failure in OOD detection (Nalisnick et al., 2019).

Normalizing Flows (NFs) as likelihood-based generative models with tractable likelihood appear to be well-suited for addressing the OOD detection problem. However, their likelihood does not provide a significant distinction for OOD data. In fact, NFs tend to assign high likelihood to OOD data (Nalisnick et al., 2019; Kirichenko et al., 2020). Therefore, it has been stated that they learn local transformations instead of semantics. This problem is fundamental because estimating the likelihood in high-dimensional spaces is

Abbreviations: **AR**, Auto-Regressive; **AUROC**, Area Under the Receiver Operating Characteristic Curve; **BPD**, Bit-Per-Dim; **DNF**, Denoising Normalizing Flow; **MSE**, Mean Squared Error; **NF**, Normalizing Flow; **NLL**, Negative Log-Likelihood; **OOD**, Out-Of-Distribution; **IC**, Input Complexity; **ID**, In-Distribution; **VAE**, Variational Auto-Encoder.

*Corresponding author.

Email addresses: `razavi_f@ut.ac.ir` (Seyedeh Fatemeh Razavi), `mahdi.mehmanchi@ut.ac.ir` (Mohammad Mahdi Mehmanchi), `reshad.hosseini@ut.ac.ir` (Reshad Hosseini), `tavassolipour@ut.ac.ir` (Mostafa Tavassolipour)

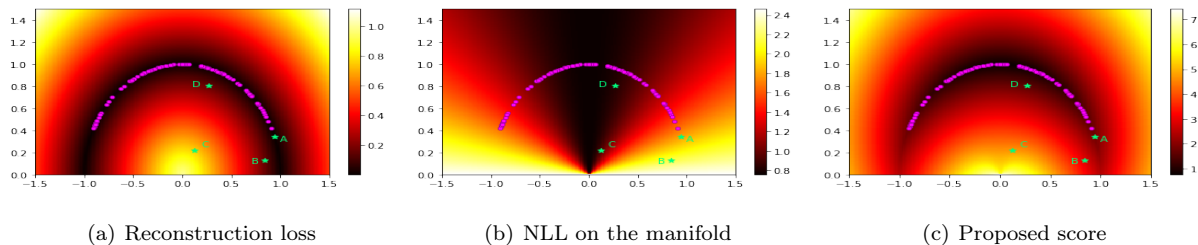
challenging (Theis et al., 2016). Using alternative measurement instead of pure likelihood is a candidate solution followed by researchers such as likelihood ratio (Ren et al., 2019), likelihood regret (Xiao et al., 2020), and Input Complexity (IC) (Serrà et al., 2020). To the best of our knowledge, the role of manifold learning to tackle the aforementioned problem has not yet been studied for NFs.

The important structural limitation of common NFs is that they cannot learn the embedded manifolds of the data. Real data are usually embedded in low-dimension manifolds, and powerful generating models use this intuition (Kingma & Welling, 2014; Goodfellow et al., 2014). NFs use bijective transformation, and therefore they preserve dimensionality between the input and transformed spaces. One can think that this can be easily solved by using non-bijective transformation that can transform the data space to a lower dimensional one, and maximizing the likelihood of the data on the low-dimensional manifold is obtained by such a transformation. But unfortunately, this optimization problem cannot be solved exactly; as is the case with some other well-known likelihood-based methods on the manifold that approximate a lower-bound of the likelihood (Kingma & Welling, 2014).

Recently, several researchers proposed solutions to the problem of maximizing the likelihood of the data on a manifold using NFs. Some use an injective transformation in NFs (Brehmer & Cranmer, 2020; Caterini et al., 2021; Huang et al., 2021). Using injective transformations makes the optimization computationally expensive. Brehmer & Cranmer (2020) used two-step training procedure, first the manifold is learned using an NF, then the density is estimated using another NF. This procedure simplifies the training, but it can lead to poor density estimation. Since, learning only the manifold during the first training step while ignoring the density estimation objective raises suspicions about acquiring a manifold that introduces difficulties and sometimes irreparable challenges in density estimation during the second training step. Horvat & Pfister (2021) introduced a method that learns a low-dimensional manifold from NFs in a single-step training procedure without using injective transformations. First, the learning of the manifold coupled with density estimation is achieved using an NF. This is followed by another NF that accurately estimates the density on the learned manifold. This procedure enhances the awareness of manifold learning along with density estimation, which distinguishes it from Brehmer & Cranmer (2020).

Inspired by the previously mentioned methods, we provide an approach to overcome the aforementioned inherent shortcoming of NFs as a likelihood-based generative model to estimate a manifold, particularly in high dimensions. Then, we employ the model for OOD detection. Fig. 1 is a toy example that illustrates the intuition behind our proposed method. Suppose that we have a semicircle dataset with unit radius where the data points are generated according to a truncated Gaussian distribution $\mathcal{N}(\mu = \frac{\pi}{2}, \sigma = 0.85, a = \frac{-\pi}{1.7}, b = \frac{\pi}{1.7})$. The data in this two-dimensional representation clearly resides on a one-dimensional manifold (i.e., a straight finite line). To find this line, for every $x \in \mathbb{R}$ and $y \in \mathbb{R}^+$, we can project point (x, y) to θ , where $0 \leq \theta \leq \pi$. By using the equations $x' = \cos(\theta)$ and $y' = \sin(\theta)$, we can then transform this line back to the semicircle and obtain the reconstructed point (x', y') . If the initial point (x, y) lies on the arc, then $(x', y') = (x, y)$. Otherwise, (x, y) will be mapped to the nearest point (x', y') on the arc. So, we can define a reconstruction

Fig. 1 A semicircle toy dataset to illustrate the proposed score for OOD detection. The score is a combination of the NLL and a measure of distance to the manifold (reconstruction loss).



loss between each point and its reconstructed point based on a distance function. Fig. 1(a) shows the reconstruction loss for points on a grid, where we used the Mean Squared Error (MSE) loss (square Euclidean distance). The NLL on the manifold for points on the grid is shown in Fig. 1(b). Now consider points A and C . Point A has low likelihood and point C has high likelihood (see Fig. 1(b)). If we only consider the likelihood on the manifold, we may incorrectly consider A an OOD sample and C an In-Distribution (ID) sample. To address this issue, we add the reconstruction loss to the NLL term with a positive constant factor. This way, our OOD score includes both the NLL and the reconstruction loss. We have presented the proposed OOD score in Fig. 1(c). Based on the provided example, it may be tempting to use only the reconstruction loss for OOD detection. However, we should consider points B and D to fully understand the importance of the likelihood term. Although points B and D have the same reconstruction loss, point D is near a region with a high density, unlike point B . Therefore, it is reasonable to consider point D as an ID sample and point B as an OOD sample. In other words, we can tolerate a bigger reconstruction loss for samples near high-density regions compared to those near low-density regions. This intuition can be clearly observed in Fig. 1(c).

To jointly estimate the density and learn the manifold, the objective would be to optimize the likelihood within the on-manifold region while imposing penalties on the off-manifold region. To achieve this, a penalty function is employed, which encourages the inverse mapping to reconstruct the original data only based on the on-manifold subspace. We combine the achieved NLL and the manifold score (reconstruction loss) to create an OOD detection score. We find this approach promising as it enhances the performance of common NFs in OOD detection tasks without increasing architectural complexity or using auxiliary OOD training data. Accordingly, our main contributions are summarized as follows:

1. We explore the impact of incorporating manifold learning into NFs for OOD detection and demonstrate that the use of NFs with manifold learning can enhance OOD detection in some cases.
2. While manifold learning with NFs algorithms typically employs the MSE penalty function, we also investigate the impact of using the Huber penalty function (Huber, 1964) during the manifold learning phase on OOD detection.

The paper is arranged as follows. Section 2 reviews the recently proposed methods related to manifold

learning in NFs and OOD detection. The preliminaries are introduced in Section 3. Section 4 introduces the proposed method. Experimental results are presented in Section 5. In the end, the conclusion is discussed in Section 6.

2. Related Work

Studies on manifold learning in NFs methods and OOD detection methods are provided in Section 2.1 and Section 2.2, respectively.

2.1. Manifold learning in NFs

This section provides a brief overview of the most relevant research about the manifold learning in NFs. In general, the methods are categorized into two classes: NFs on prescribed manifolds and NFs on learnable manifolds. The first class focuses on learning flows on prescribed manifolds, while the second one includes learning the manifold, which aligns closely with our study. We discuss the most related research in the second category in the next.

Recently, solutions to the problem of manifold learning and density estimation with NFs have been proposed (Kim et al., 2020; Kothari et al., 2021; Huang et al., 2021; Brehmer & Cranmer, 2020; Caterini et al., 2021; Horvat & Pfister, 2021; Kalatzis et al., 2022; Ross & Cresswell, 2021). In the following, we review the most related works to our research and highlight their key properties. A proposed scientific path is about separating manifold learning and density estimation. The pioneer of this study in NF is a method named \mathcal{M} -flow (Brehmer & Cranmer, 2020). In \mathcal{M} -flow, an injective NF transformation is used to transform the data into a manifold. After that, another NF is used to estimate the density on the manifold. Manifold learning and density estimation are done separately to avoid the computation of Jacobian term induced by the injective transformation (two-phase training). An extension of this study called multi-chart flow (Kalatzis et al., 2022), which employs multiple mapping instead of one to find a manifold with multiple charts. It also suffers from two-phase training. Another followed research of \mathcal{M} -flow, named Rectangular flow (Caterini et al., 2021), overcomes the calculation of injective transformation by relying on automatic differentiation and linear algebra tricks. A recent study, named Denoising NF (DNF) (Horvat & Pfister, 2021), overcomes the limitations of using injective transformations and separating model training by splitting the transformed space of an NF into two parts, noise-insensitive and noise-sensitive. These parts are modeled by another NF and a low-variance Gaussian distribution, respectively. The noise is also added to the input training data. Using this structure, two-phase training is no longer needed and the two NFs are trained simultaneously.

2.2. Out-of-distribution detection

A brief overview of recent and prominent developments in OOD detection is provided in the following. It should be noted that while there is a wide range of topics for this discussion (Yang et al., 2022), the main focus of the current research is OOD detection through density estimation.

Non-density-based methods.

Contrary to the main focus of this paper, OOD detection methods are not limited to density-based models. Using data labels can be a guide for this problem. Applying an appropriate threshold on a pre-trained classifier, decreasing the model’s overconfidence, changing the training approach, and using an auxiliary OOD training data are common approaches (Lee et al., 2018; Hendrycks et al., 2019; DeVries & Taylor, 2018; Liang et al., 2018).

Lee et al. (2018) proposes a pre-training algorithm by using generated auxiliary OOD training data. Since classifiers are not trained for the purpose of OOD detection, but instead to increase accuracy in inference time, a targeted pre-training approach can help the model enrich its features and decrease the model’s confidence in OOD data. Same to the mentioned research, one of the related researches (called outlier exposure) defines a specific loss function to discriminate between ID data and an auxiliary OOD data with a ranking loss to enhance the pre-training approach (Hendrycks et al., 2019). Confidence estimation along with the main objective function (DeVries & Taylor, 2018) or using a temperature-based Softmax function (Liang et al., 2018) are other solutions pursued in the literature.

Density-based methods.

It seems likelihood-based generative models can be good candidates for OOD detection by assigning less probability to OOD data. However, a frequent point about likelihood-based models such as Auto-Regressive (AR) models (Ren et al., 2019), Variational Auto-Encoders (VAEs) (Xiao et al., 2020), and NFs (Nalisnick et al., 2019; Kirichenko et al., 2020) is that the likelihood is not a distinguishing score for OOD data (Zhang et al., 2021; Nagarajan et al., 2021). The common weakness of all the mentioned models is that they also learn the background and irrelevant information. In other words, they equally attend to whole space.

Using the likelihood ratio instead of pure likelihood in AR models is a well-known solution that was proposed for the first time to solve the sequential genomics OOD detection (Ren et al., 2019). It considers a background/semantic decomposition of data. The ratio score is obtained by dividing the likelihood value of the model by the likelihood value of a background model. The background model is trained by perturbing data to learn the background information. The defined ratio implicitly ignores irrelevant information. Despite the success of this model in genomic OOD detection, it has not achieved state-of-the-art results on image datasets. A remarkable solution for VAE is named likelihood regret (Xiao et al., 2020). This method is based on the principle that OOD data can drastically shift the likelihood after several fine-tuning steps. The authors employ a VAE to avoid overfitting in fine-tuning steps with freezing the decoder block.

According to the literature, NFs only learn local transformations rather than semantics (Nalisnick et al., 2019; Kirichenko et al., 2020). Therefore, despite having tractable likelihood, they suffer from shortcomings in OOD detection. Previously proposed methods try to integrate high-level information in any way to avoid the OOD fault. At first, the results of training NFs on the embedded data instead of raw one confirm this claim (Kirichenko et al., 2020). Moreover, improving OOD detection can be achieved by redesigning the model’s architecture. Using attention units (Kumar et al., 2021) or deep residual flows (Zisselman & Tamar, 2020) can

be mentioned as pioneer works. Same to non-density-based methods, changing training strategies (such as using information theory (Ardizzone et al., 2020)) can be effective for OOD detection. Employing a test-time OOD score based on input complexity is a valuable measurement (Serrà et al., 2020). It is considered as a likelihood ratio between the learned density and a universal lossless compressor. Simple data are coded in fewer bits. So, the ratio between the trained model and the compressor achieves a likelihood ratio to reach the actual number of bits. A line of research overcomes this limitation by ensembling models (Choi et al., 2019). Surprisingly, this approach was successful despite its over-parametrization. Although every density estimation model is not able to make an accurate diagnosis, but the mentioned research shows that the combination of such models in aggregate form is successful contrary to expectations.

Best of our knowledge, investigating the effect of manifold learning in NFs on OOD detection has not been covered in the literature.

3. Preliminaries

This section introduces our notations and related preliminary works to make it easier for the reader to follow the subject. The rest of this section is arranged as follows: At first, the standard normalizing flow is discussed in Section 3.1. After that, a robust reconstruction loss function is presented in Section 3.2.

3.1. Normalizing Flow

There are a variety of well-known deep likelihood-based generative methods, like VAEs (Kingma & Welling, 2014), NFs (Rezende & Mohamed, 2015), AR models (Murphy, 2022), energy base models (Murphy, 2022), and diffusion models (Sohl-Dickstein et al., 2015). But among the mentioned models, only ARs and NFs can exactly compute the likelihood. VAEs and diffusion models find a lower bound on the likelihood, while energy base models approximate it. Sampling in common AR models is computationally expensive, due to sequential nature of these models. Sampling in NFs is not sequential, but they have a structural limitation (dimension-preserving) that limits their applicability and generating power.

NF is a parametric diffeomorphism transformation, $f_\phi : \mathbb{R}^D \rightarrow \mathbb{R}^D$. So, it is a two-side differentiable bijective transformation. By choosing a random variable from a pre-defined distribution in $Z \in \mathbb{R}^D$ and transferring back it by f_ϕ^{-1} , the distribution of data can be found by a change-of-variable formula like

$$p_X(X) = p_Z(f_\phi(X)) |\det J_{f_\phi}(f_\phi(X))|, \quad (1)$$

where $J_{f_\phi} \in \mathbb{R}^{D \times D}$ is the Jacobian matrix of the transformation f_ϕ . It is clear that the practical computability constraint for this term is the implicit constraint imposed on NFs. Moreover, the model parameters are estimated by the NLL criterion

$$\phi^* = \arg \min_{\phi} (-\log p_X(x)), \quad (2)$$

where $x = \{x_n\}_{n=1}^{n=N}$ is the available training data from the distribution p_X .

3.2. Reconstruction loss functions

During the training of NFs on a manifold, all off-manifold data have a likelihood of 0. In the literature, penalizing the off-manifold part through a quadratic reconstruction function, typically MSE, is a common approach to addressing this problem (Brehmer & Cranmer, 2020; Caterini et al., 2021; Horvat & Pfister, 2021; Ross & Cresswell, 2021). A weakness of quadratic functions is its sensitivity to off-manifold data points. However, a regularized reconstruction function utilizes both linear and quadratic functions, with the function type changing depending on a comparison between the error value and a threshold δ . Accordingly, this switching leads the off-manifolds are not penalized as much as on-manifold data.

Eq. 3 defines a switching function named the Huber function (Huber, 1964) with a strong background in robust statistics.

$$H_\delta(x, y) = \begin{cases} 0.5(x - y)^2, & \text{if } |x - y| < \delta \\ \delta(|x - y| - 0.5\delta), & \text{otherwise} \end{cases} \quad (3)$$

4. Proposed method

By considering a standard NF like f_ϕ , the density of data is estimated by Eq. 1. It would be exciting if we could calculate the density of data on the manifold and measure its impact on OOD detection. However, density estimation on manifolds is not easy. In this paper, we take inspiration from existing methods of manifold learning in NFs (\mathcal{M} -flow (Brehmer & Cranmer, 2020) and DNF (Horvat & Pfister, 2021)) and propose a new one to detect OOD data.

From the manifold perspective, the transformed (or latent) space (z) can be disentangled into two spaces, on-manifold (u), and off-manifold (v) space. This is because placing all real-value data on a manifold is not necessarily a correct assumption, and some of the data is generally outside the manifold. The distribution of the transformed data is a joint distribution of these two parts like $p_Z(z) = p_Z(u, v)$. With assuming independence among two spaces $u \perp v$, the distribution of the transformed space is decomposed into the product of two sub-space’s distributions as $p_Z(z) = p_U(u) \times p_V(v)$, where $U : \mathcal{M}_M \subseteq \mathbb{R}^d$ and $V : \mathcal{M}_O \subseteq \mathbb{R}^{D-d}$ are the on-manifold and the off-manifold sub-spaces, respectively.

Our goal is to rearrange the transformed space of an NF in such a manner that a portion corresponds to the on-manifold part, while the other corresponds to the off-manifold part. Let $f_\phi : \mathbb{R}^D \rightarrow \mathbb{R}^D$ be a standard NF. We denote the first d components of the output of f_ϕ as u and the remaining ones as v where u stands for an on-manifold part of data and v for an off-manifold part. Formally, $z = f_\phi(x) = (z_1, z_2, \dots, z_D)$, $u = (z_1, z_2, \dots, z_d)$, $v = (z_{d+1}, z_{d+2}, \dots, z_D)$, where x is the input, and z is the corresponding transformed data by the NF. We choose $p_Z(z) = \mathcal{N}(0, I_D)$ and factorize $p_Z(z)$ such that $p_Z(z) = p_U(u) \times p_V(v)$.

It should be mentioned that we can use another NF h_θ to fit a more complex distribution on the on-manifold part (u) rather than a Gaussian distribution. This idea was followed by DNF (Horvat & Pfister, 2021) and \mathcal{M} -flow (Brehmer & Cranmer, 2020) for density estimation. Briefly, in this case, $p_U(u)$ is replaced by $p_{U'}(u') |\det G_{h_\theta}(u')|$, where u' is the transformed space by $h_\theta : \mathbb{R}^d \rightarrow \mathbb{R}^d$, and $p_{U'}(u') = \mathcal{N}(0, I_d)$. Moreover,

DNF fits a tight Gaussian distribution $p_V \sim \mathcal{N}(0, \epsilon I_{D-d})$ on the off-manifold part based on the added noise value ϵ to the data. However, the influence of the added noise in DNF was not reported to have a significant effect. This is likely because the model is trained on real-valued data that have inherent quantization noise, making the addition of more noise unnecessary. Consequently, we do not add noise to data in our framework, and so there are some minor differences with DNF.

The mentioned changes on standard NFs are not sufficient for manifold learning. It is necessary to penalize the off-manifold sub-space so that the model is able to reconstruct the data from the on-manifold sub-space. Accordingly, a constrained optimization problem on NLL appears like

$$\min_{\phi} \text{NLL}(x; \phi) \text{ s.t. } \mathcal{C}(x, \tilde{x}) \leq \tau, \quad (4)$$

where $x = (x_1, x_2, \dots, x_D)$, $\tilde{x} = (\tilde{x}_1, \tilde{x}_2, \dots, \tilde{x}_D) = f_{\phi}^{-1}(\text{proj}(f_{\phi}(x)))$, \mathcal{C} , and τ are the input data, corresponding reconstruction (computed through the inverse of normalizing flow f_{ϕ}), the penalty function, and the penalization threshold, respectively. Moreover, $\text{proj}(f_{\phi}(x))$ is the first d components of $f_{\phi}(x)$ corresponding to the data manifold, padded with zero as $\text{proj}(f_{\phi}(x)) = (u, \vec{0}_{D-d})$.

Existing methods such as \mathcal{M} -flow (Brehmer & Cranmer, 2020), DNF (Horvat & Pfister, 2021), and Rectangular flow (Caterini et al., 2021) penalize the off-manifold with a quadratic constraint. An important characteristic of a quadratic function is its sensitivity to outliers, that can be interpreted as off-manifold parts of the data. One aspect of our contribution involves using a switching penalization function, containing both linear and quadratic forms, which is determined based on the distance to the manifold. The switching is modeled with a Huber function (Eq. (3)). In the proposed method, an element-wise Huber function with threshold δ , denoted H_{δ} , is applied to the difference between the input data (x) and the reconstructed one (\tilde{x}). The reconstructed data is a function of manifold ($\tilde{x} = f_{\phi}^{-1}(\text{proj}(f_{\phi}(x)))$) rather than joint on-manifold and off-manifold parts. Therefore, the penalization term is computed by averaging an element-wise function like

$$\mathcal{C}(x, \tilde{x}; \delta) = \frac{1}{D} \sum_{i=1}^D H_{\delta}(|x_i - \tilde{x}_i|, 0). \quad (5)$$

Inspired by the Lagrange multipliers method, the proposed constrained optimization problem can be converted to its unconstrained equivalent one

$$\ell = -\log P_u(u) - \log P_v(v) + \log |\det J_{f_{\phi}}(x)| + \lambda \mathcal{C}(x, \tilde{x}; \delta), \quad (6)$$

where λ is the penalization term hyper-parameter, and the first three terms are the objective of a standard NF (called NLL).

The proposed approach not only facilitates the estimation of manifold density for NFs but also addresses the limitations of relying solely on likelihood or reconstruction for OOD detection, as extensively explained in Section 1 (see Fig. 1). In other words, high likelihood or low reconstruction error alone are not reliable indicators for identifying ID data. However, by combining these two factors using the introduced cost function (Eq. 6), we not only estimate the manifold using NFs but also introduce an appropriate indicator for OOD detection that is validated through comprehensive experiments.

5. Results

The primary goal of the experiments is to explore the significance of manifold learning in NFs for enhancing OOD detection. Moreover, the performance of the proposed method is also evaluated in terms of image generation because it is fundamentally a generative model. As previously mentioned, \mathcal{M} -flow (Brehmer & Cranmer, 2020) and DNF (Horvat & Pfister, 2021) are existing methods that closely resemble our approach for manifold learning in NFs. Our proposed OOD detection score, combines the precise likelihood value with the reconstruction loss. However, \mathcal{M} -flow cannot effectively achieve high-dimensional likelihood due to using injective transformations. Therefore, our focus is on comparing our approach with the DNF framework in terms of image generation performance. Subsequently, we compare our OOD detection results with some other state-of-the-art likelihood-based OOD detection methods such as likelihood ratio (Ren et al., 2019) and IC (Serrà et al., 2020). All in all, we observed that penalizing the learned manifold in the proposed method leads to consider the dominant manifold as the ID manifold and the remains (like less frequent details) as OOD regions.

5.1. Experimental setting

The used dataset and experimental setting are described in Section 5.1.1 and Section 5.1.2, respectively.

5.1.1. Dataset

The seven used datasets in the current study are introduced in Table 1. We could increase the number of layers and parameters in proportion to the original image’s dimensions. Still, due to resource allocation limitations, we resize the color images to 32×32 in our experiments.

5.1.2. Architecture

For two-blocks models such as standard DNF or architecture searching experiments, we use the Glow model (Kingma & Dhariwal, 2018) for f_ϕ and the RealNVP model (Dinh et al., 2017) for h_θ . Meanwhile, for one-block models, we use either one of the models. Our Glow model has three blocks, each with 32 steps of the flow. Each step consists of an actnorm layer, an invertible 1×1 convolution layer, and an affine coupling layer (see Kingma & Dhariwal (2018) for the details of each layer). There is also a squeeze layer before each step and a split layer after each step. The RealNVP model comprises six affine coupling layers and six masking layers before each affine coupling layer. While DNF has chosen a specific architecture in its experiments, the employed architectures in this paper are based on two well-known NFs, Glow and RealNVP. Our main goal is to show the importance of manifold learning in NFs for OOD detection, regardless of the specific architecture.

5.1.3. Training

All implementations are done in the PyTorch¹(version 1.10.0+cu102) framework. We use Adam (Kingma & Ba, 2015) as our optimization algorithm with a learning rate of $1e-5$ and a batch size of 64. Also, we set

¹<https://pytorch.org/>

Table 1 The information of the used datasets in the paper.

Data	Description
MNIST (LeCun & Cortes, 2010)	Containing a set of 28×28 gray-scale hand-written digit images in 10 classes (50k training images, 10k test images)
FMNIST (Xiao et al., 2017)	Including a set of 28×28 gray-scale fashion products images from 10 different categories (60k training images, 10k test images). The dataset’s original title is Fashion-MNIST, which we abbreviate as FMNIST.
SVHN (Netzer et al., 2011)	Consisting of 32×32 RGB house number plates (about 73k training images and 26k test images)
CIFAR10 (Krizhevsky et al., 2009)	Containing 60k 32×32 RGB images of 10 categories (50k training images, 10k test images)
CelebA (Liu et al., 2015)	Consisting about 200k face images of 10,177 persons (180k training images, 20k test images). A resized version (32×32) is used in this paper.
LSUN (Yu et al., 2016)	Including a variety of large-scale images categorized into 10 classes. In this study, we only used bedroom class images. This class comprises more than 3 million images in the original dataset, but we use only about 300k 32×32 resized version of them.
Constant	A manual created dataset of 60k 32×32 constant color images (50k training images, 10k test images)

the value of the penalization term coefficient (λ) to 100. All training experiments were done on a single GPU (GTX 1080 Ti), with Cuda version 11.4 and 11019GB memory. The implementation codes of the proposed methods are attached to this file.

5.2. Architecture searching

In this section, we consider four structures: DNF, MSE-based off-manifold penalization with two blocks (called Proposed-M), Huber-based off-manifold penalization with two blocks (called Proposed-H), and Huber-based off-manifold penalization with one block (called Proposed-D). In the first three, two NFs (named f_ϕ and h_θ , Glow followed by RealNVP) are used, and in the last structure, a single NF (named f_ϕ) is used. Briefly, we employ two blocks together as an NF to be more comparable in structure with DNF. Therefore, the two-blocks method means using a dimension preserving NF (RealNVP in our setting) to estimate the density of the manifold part (same as DNF) instead of the Gaussian distribution. We choose all DNF backbone models the same as ours in all experiments for a fair comparison.

We only present the results of CelebA here and the rest are available in the supplementary files. Based on the reported results for CelebA dataset by Horvat & Pfister (2021) (DNF), we consider $d = |\mathcal{M}_M| \sim 500$

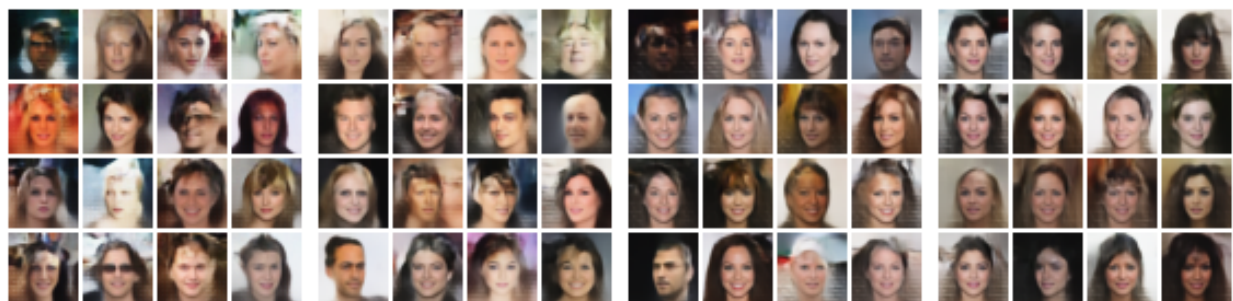
for architecture searching. It is worth noting that, we assume prior knowledge of the manifold’s intrinsic dimension from existing works in the field. Our goal is not to determine the intrinsic dimension of the manifold. Readers seeking dimensionality determination can refer to Horvat & Pfister (2022) and Pope et al. (2021)

The results of experiment on CelebA dataset are shown in Table 2 and Fig. 2. The main goal of the designed experiment is to find an appropriate architecture for generating data from the manifold as long as it does not decrease the likelihood of data. The reported results in Table 2 confirm that our proposed methods (Proposed-H, Proposed-M, and Proposed-D) outperform DNF in terms of Bit-Per-Dim (BPD) (calculated by $\frac{NLL}{D \times \log 2}$), whereas their generated images look visually similar, according to Fig. 2. An important aspect of DNF is its reliance on incorporating noise during training. It is noteworthy that the reported inference BPD for the DNF is computed using noiseless data, and making it an approximation. It is worth mentioning that best generated images in Horvat & Pfister (2021) (DNF) are based on a well-defined StyleGAN manifold (Karras et al., 2020), not on raw data. Additionally, their reported generated images on the CelebA dataset are not visually perfect.

Table 2 The best MSE/BPD scores for data lie in $\mathcal{M} \subset \mathbb{R}^{500}$. Dimension changing of the one-block (Proposed-D) and two-block (DNF, Proposed-M, Proposed-H) methods are $\mathbb{R}^{3072} \rightarrow \mathbb{R}^{500}$ and $\mathbb{R}^{3072} \rightarrow \mathbb{R}^{500} \rightarrow \mathbb{R}^{500}$. #Params means the number of trainable parameters.

Criterion	DNF	Proposed-M (two-block)	Proposed-H (two-block)	Proposed-D (one-block)
MSE	0.004 ± 0.0002	0.005 ± 0.0003	0.01 ± 0.001	0.02 ± 0.001
BPD	3.98 ± 0.03	3.52 ± 0.04	3.51 ± 0.04	3.52 ± 0.04
#Params	$\approx 59M$	$\approx 59M$	$\approx 59M$	$\approx 44M$

Fig. 2 Generated CelebA images corresponding to experiments in Table 2.



(a) DNF

(b) Proposed-M

(c) Proposed-H

(d) Proposed-D

Moreover, since the Huber function applies a linear function to penalize the off-manifold pixels rather than a quadratic one, we anticipated that the MSE would be higher in the models that were penalized with the Huber function. In addition to the aforementioned factors, the integration of reconstruction loss and BPD

value is a crucial component in our study. Although the reconstruction loss may slightly lag behind the DNF method in Table 2, our approach does not just depend on reconstruction or BPD (as scaled NLL) for OOD detection. Based on the evaluation of the results in the latter three columns, we can confidently assert that the proposed method offers a promising advantage in this regard. Another strength is that the Proposed-D method achieves same images (in terms of visual quality in Fig. 2) to DNF and other two-blocks proposed methods, with fewer parameters while maintaining the likelihood. Considering the outcomes, the proposed-D model is chosen for further experiments in the following. To summarize, we use the term "proposed" to denote the model referred to as "proposed-D".

By choosing Proposed-D as the base model, more experiments are presented here to evaluate the performance of the model in terms of generation and manifold learning on ID/OOD data. The order of experiments is in such a way that the ability of the models is measured for different ID/OOD data and different manifold dimensions (10, 50, 100, 500, 1000). The results for CelebA test data are presented here. The results of other datasets are available in the supplementary file.

Fig. 3 contains the generated and reconstructed data (learned manifold) for a model trained on CelebA. In low-dimensional manifolds, images generated by the model are limited to displaying the main manifold of the face and the background details are not generated. However, as the manifold dimensions increase, the inclusion of less frequent details (mostly related to the background) in the generated image is observed. If the data manifold has simplistic visual attributes (e.g., as observed in the SVHN dataset results presented in the supplementary file), the likelihood can be better fit to the data, and thus sharpened images can be generated as manifold dimension increases. This trend is also observed in more complex datasets such as CIFAR10 (as noted in the supplementary file) when the likelihood is fitted using various dimensions of the manifold.

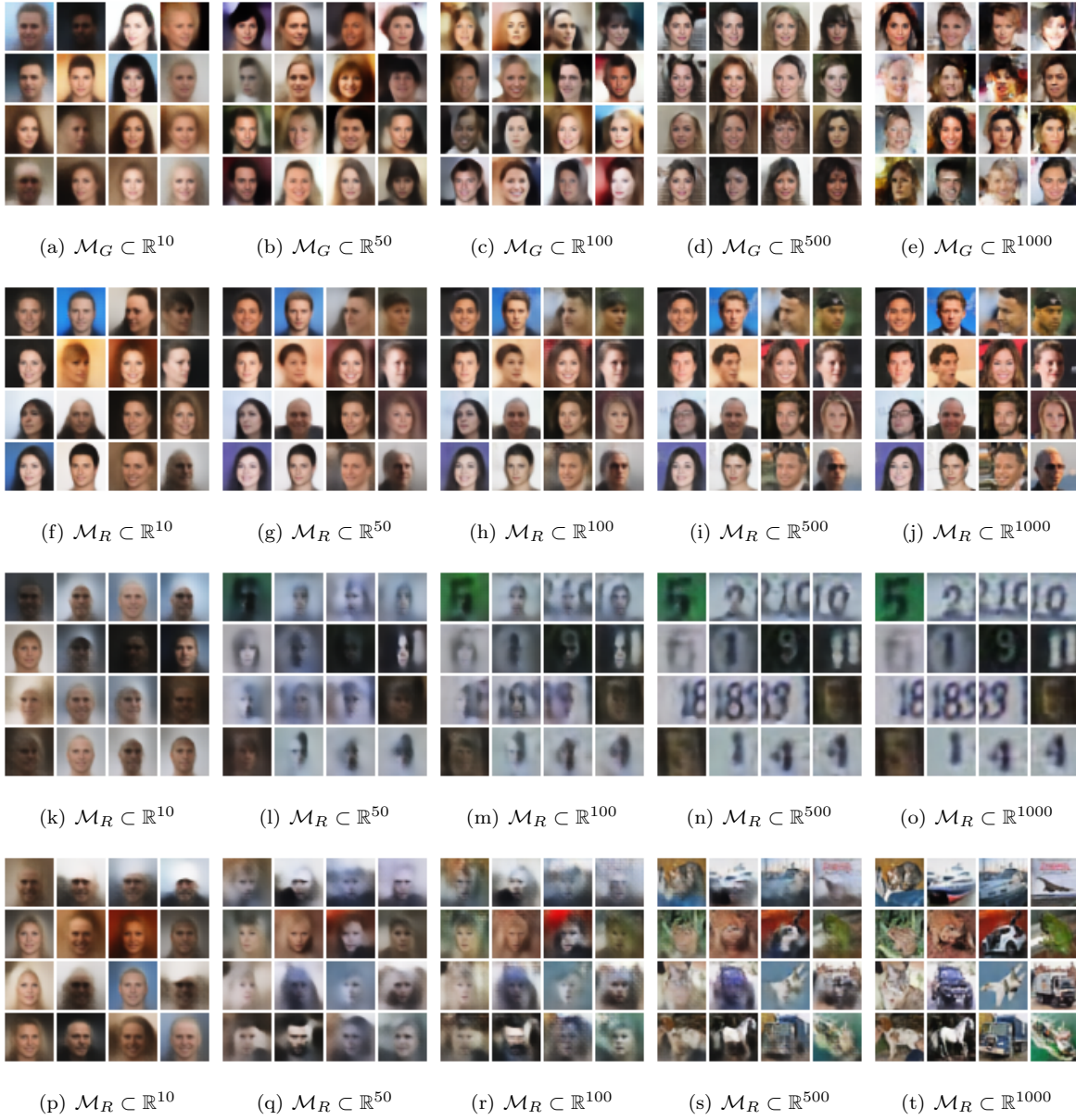
The second row of Fig. 3 contains the reconstruction of CelebA test data on the model trained with CelebA for the corresponding manifold dimension. The reconstruction ability is improved by increasing the dimension. As it is clear, the model's invertibility power will appear by increasing manifold dimension, the same as standard NF. The model trained on CelebA not only excels at generating and reconstructing ID data but also demonstrates great performance in discriminating OOD data. In case of reconstructing OOD data in third and fourth rows of Fig. 3, especially from low dimensions, it cannot reconstruct OOD data well. In other words, learning low dimension manifold for ID data leads to focusing on ID specific features instead of global features. It is worth noting that our point is about manifold learning while in case of dimension preserving (like standard NFs), the reconstruction is done without error.

5.3. Image OOD detection

In this section, we present the results of OOD detection for gray-scale images, and we also expand our analysis to include high-dimensional color images and hyper-parameter (d and δ) search.

At first, the pre-defined RealNVP is employed as a backbone model for manifold learning and OOD detection of gray-scale images. The purpose of the designed experiment is to evaluate the performance of various penalty functions in cases where distinguishing between ID and OOD data becomes challenging due

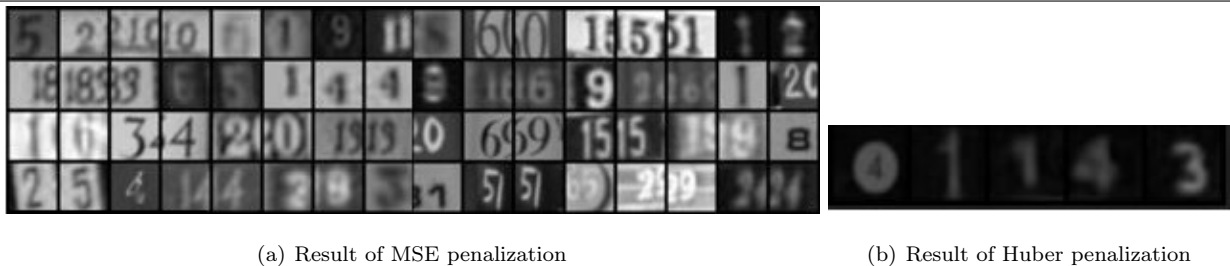
Fig. 3 Several generated (first row) and reconstructed images (CelebA as ID data in the second row, SVHN and CIFAR10 as OOD data in the third and forth rows, respectively) from the proposed-D method for different manifold dimensions (10, 50, 100, 500, and 1000 from left to right) for a model trained on the CelebA dataset. $\mathcal{M}_G \subset \mathbb{R}^d$ and $\mathcal{M}_R \subset \mathbb{R}^d$ represent image generation and image reconstruction from a manifold fall in dimension d , respectively.



to visual similarity. The model is trained on the MNIST dataset as ID data with an embedded manifold in \mathbb{R}^3 . Then, it is evaluated with 28×28 gray-scale SVHN as OOD data. A hard OOD detection threshold is determined as the maximum score obtained from the MNIST test data. Any sample with higher score than this threshold is classified as OOD data. The reported results in Fig. 4 confirm the considerable superiority of using the Huber function compared to MSE in successfully identifying OOD data with high overlap.

Based on Fig. 4, the Huber function exhibits significantly fewer mistakes on the SVHN test data compared to MSE. Furthermore, the mistakes made by the Huber function are more meaningful, particularly in situations where the data visually resembles the ID data (MNIST). To provide further clarification, the Huber function nearly almost tends to make errors on images resembling data within a distribution that consists of a single digit on a dark background. It is important to highlight that MNIST is structured in such a manner that each image contains a single digit placed on a black background. Nevertheless, when the data deviates from this pattern, as seen in cases like SVHN (including house license plate numbers) where multiple digits may appear in a single image, the Huber function may exhibit fewer errors. On the other hand, the MSE function exhibits a higher number of errors and even mistakenly recognizes images containing multiple digits as ID data.

Fig. 4 All misdetected ID 28×28 gray-scale SVHN test data for a trained model on MNIST.



The effect of manifold learning on color image OOD detection for NFs in comparison with other methods (Kingma & Dhariwal, 2018; Ren et al., 2019; Serrà et al., 2020) is evaluated in terms of AUROC (Area Under the Receiver Operating Characteristic Curve) criterion in Table 3 (trained on SVHN), Table 4 (trained on CIFAR10), and Table 5 (trained on CelebA). AUROC computes the area under the ROC curve by using un-thresholded normalized predictions to the range of $[0, 1]$ on the data along with binary true labels. In our configuration, we assign a true label of 0 for ID data and a true label of 1 for OOD data. A higher AUROC value indicates better performance.

The most important reason behind selecting the methods for comparison in Table 3, Table 4, and Table 5 is their consistency in the assumptions with our proposed method, meaning that auxiliary OOD training data is not employed, and the model structure is not tuned for this task, despite still achieving state-of-the-art results. Each reported table consists of two separate parts (first for the Huber and the next for MSE penalization). The first column includes the name of the OOD data used during testing. The next columns are associated with different manifold dimensions. In the case of dimension-preserving ($d = D$), the baseline method (Kingma & Dhariwal, 2018) (reported architecture in Section 5.1.2), the likelihood ratio method (Ren et al., 2019)

(with the same architecture as reported Glow network in Section 5.1.2), and the input complexity method (Serrà et al., 2020) (with the same architecture as reported Glow network in Section 5.1.2) are evaluated. The next columns for different manifold dimensions have the same partitioning: the proposed method (named P), the proposed method with considering likelihood ratio (named P + ratio), and the proposed method with considering input complexity (named P + IC). To summarize the approach of combining the proposed method with the two mentioned methods (likelihood ratio and input complexity), it can be stated that, based on the details provided in Section 2, as both methods are test time scores, we incorporate only the compressor loss from the input complexity method and the background loss from the likelihood ratio method into our score.

Table 3 shows the superiority of the proposed method for different manifold dimensions in complicated datasets. However, for simple-manifold family datasets, the combination of the proposed method and IC is more effective. Additionally, the performance of the proposed method appears to be nearly indistinguishable when using both types of penalty functions. The Huber function only demonstrates a slight advantage over MSE in very low dimensions. In short, regardless of the specific penalty function used, the concept of proposed method demonstrates some advantageous in OOD detection. The presented results in Table 4 and Table 5 demonstrate similar performance to those in Table 3. The key difference is that the proposed method alone or its combination with the two mentioned methods (ratio, IC) outperform the likelihood ratio and IC methods in terms of AUROC.

At end, one notable observation derived from analyzing the outcomes of the trained model on the SVHN dataset, which can be generalized to other datasets, is the effect of adjusting the parameters d and δ on the AUROC value. These results emphasize the significance of δ and d in determining the model’s performance, as depicted in Fig. 5.

The left figure in Fig. 5 illustrates the changes in the model’s performance as δ is increased. The mean and standard deviation reported for each δ are based on models trained with that specific threshold but with varying values of d . It is obvious that increasing δ leads to higher AUROC values for datasets with simpler data manifolds (like MNIST, FMNIST, and constant). However, the impact of δ on the AUROC value appears to be unnoticeable for datasets with complex manifolds (like CelebA, CIFAR10, and LSUN). It is important to note that excessively high values of δ may deviate from the primary objective of the problem. The mean and standard deviation reported for each δ are based on models trained with that specific threshold but with varying values of d . The right plot in Fig. 5 demonstrates the effect of d on the AUROC value. Each star point on the diagram represents the mean and standard deviation of the output from trained models with different δ for a fixed d . We observe that as the dimensionality increases, the model’s ability for OOD detection decreases, particularly in datasets with simpler manifolds. However, it is clear that excessively reducing the dimensionality by choosing a value of d smaller than the actual data manifold is not suitable.

Table 3 AUROC score for Glow (Kingma & Dhariwal, 2018), likelihood ratio method (named ratio) (Ren et al., 2019), input complexity method (named IC) (Serrà et al., 2020) with a lossless PNG compressor, and all cases of the proposed method, namely the pure case (named P), including ratio (P+ratio) and including IC (P+IC). Models are trained on SVHN.

	$d = 3072$			$d = 1000$			$d = 500$		
	Glow	ratio	IC	P	P+ratio	P+IC	P	P+ratio	P+IC
Huber									
MNIST	0.662	0.588	1.0	0.722	0.369	1.0	0.873	0.391	1.0
FMNIST	0.863	0.998	1.0	0.872	0.626	0.986	0.932	0.629	0.986
Cifar10	0.99	1.0	0.408	0.991	0.286	0.079	0.992	0.287	0.08
LSUN	0.996	1.0	0.647	0.997	0.174	0.091	0.997	0.174	0.091
CelebA	0.998	1.0	0.423	0.998	0.115	0.051	0.998	0.115	0.051
Constant	0.543	0.685	1.0	0.501	0.535	1.0	0.567	0.532	1.0
MSE									
MNIST	0.662	0.588	1.0	0.751	0.375	1.0	0.916	0.433	1.0
FMNIST	0.863	0.998	1.0	0.896	0.632	0.986	0.948	0.635	0.986
Cifar10	0.99	1.0	0.408	0.991	0.289	0.08	0.993	0.291	0.08
LSUN	0.996	1.0	0.647	0.997	0.176	0.091	0.997	0.177	0.091
CelebA	0.998	1.0	0.423	0.998	0.117	0.051	0.998	0.117	0.051
Constant	0.543	0.685	1.0	0.545	0.523	1.0	0.579	0.533	1.0
	$d = 100$			$d = 50$			$d = 10$		
	P	P+ratio	P+IC	P	P+ratio	P+IC	P	P+ratio	P+IC
Huber									
MNIST	0.889	0.378	1.0	0.934	0.395	1.0	0.994	0.511	1.0
FMNIST	0.954	0.632	0.986	0.96	0.637	0.986	0.996	0.706	0.988
Cifar10	0.992	0.288	0.08	0.989	0.29	0.08	0.979	0.295	0.08
LSUN	0.996	0.175	0.091	0.993	0.176	0.091	0.985	0.179	0.092
CelebA	0.997	0.116	0.051	0.995	0.117	0.051	0.989	0.122	0.052
Constant	0.588	0.53	1.0	0.671	0.534	1.0	0.719	0.538	1.0
MSE									
MNIST	0.906	0.386	1.0	0.935	0.399	1.0	0.99	0.549	1.0
FMNIST	0.964	0.639	0.986	0.967	0.647	0.987	0.991	0.732	0.989
Cifar10	0.992	0.293	0.08	0.986	0.296	0.08	0.986	0.304	0.081
LSUN	0.996	0.179	0.091	0.991	0.18	0.092	0.978	0.187	0.093
CelebA	0.997	0.119	0.051	0.993	0.12	0.051	0.983	0.13	0.053
Constant	0.562	0.525	1.0	0.681	0.532	1.0	0.752	0.542	1.0

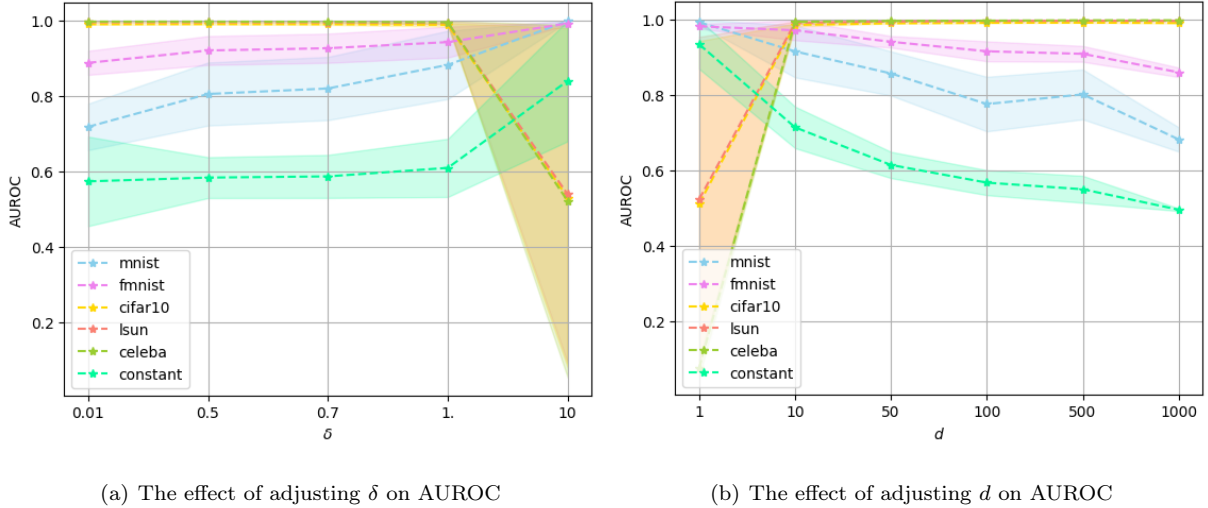
Table 4 AUROC score for Glow (Kingma & Dhariwal, 2018), likelihood ratio method (named ratio) (Ren et al., 2019), input complexity method (named IC) (Serrà et al., 2020) with a lossless PNG compressor, and all cases of the proposed method, namely the pure case (named P), including ratio (P+ratio) and including IC (P+IC). Models are trained on CIFAR10.

	$d = 3072$			$d = 1000$			$d = 500$		
	Glow	ratio	IC	P	P+ratio	P+IC	P	P+ratio	P+IC
Huber									
MNIST	0.002	0.004	1.0	0.002	0.992	1.0	0.003	0.992	1.0
FMNIST	0.016	0.014	0.999	0.021	0.937	0.997	0.025	0.938	0.997
SVHN	0.057	0.004	0.86	0.055	0.435	0.921	0.052	0.435	0.921
LSUN	0.541	0.544	0.779	0.535	0.464	0.665	0.534	0.464	0.665
CelebA	0.486	0.558	0.558	0.484	0.571	0.559	0.49	0.571	0.559
Constant	0.112	0.087	1.0	0.158	0.687	1.0	0.12	0.687	1.0
MSE									
MNIST	0.002	0.004	1.0	0.004	0.992	1.0	0.008	0.992	1.0
FMNIST	0.016	0.014	0.999	0.031	0.938	0.997	0.067	0.938	0.997
SVHN	0.057	0.004	0.86	0.054	0.435	0.921	0.046	0.432	0.921
LSUN	0.541	0.544	0.779	0.543	0.465	0.665	0.542	0.465	0.665
CelebA	0.486	0.558	0.558	0.487	0.571	0.559	0.5	0.572	0.56
Constant	0.112	0.087	1.0	0.157	0.697	1.0	0.146	0.687	1.0
	$d = 100$			$d = 50$			$d = 10$		
	P	P+ratio	P+IC	P	P+ratio	P+IC	P	P+ratio	P+IC
Huber									
MNIST	0.002	0.992	1.0	0.004	0.992	1.0	0.008	0.992	1.0
FMNIST	0.027	0.938	0.997	0.031	0.938	0.997	0.049	0.938	0.997
SVHN	0.057	0.436	0.921	0.06	0.436	0.921	0.065	0.436	0.921
LSUN	0.525	0.464	0.665	0.521	0.464	0.665	0.503	0.464	0.665
CelebA	0.494	0.571	0.559	0.495	0.571	0.559	0.511	0.572	0.559
Constant	0.256	0.691	1.0	0.293	0.695	1.0	0.416	0.718	1.0
MSE									
MNIST	0.027	0.992	1.0	0.359	0.993	1.0	0.93	0.995	1.0
FMNIST	0.122	0.939	0.997	0.317	0.942	0.997	0.857	0.951	0.997
SVHN	0.047	0.429	0.921	0.067	0.425	0.921	0.119	0.418	0.921
LSUN	0.523	0.464	0.666	0.53	0.464	0.666	0.54	0.464	0.667
CelebA	0.488	0.572	0.56	0.547	0.574	0.561	0.688	0.588	0.566
Constant	0.197	0.691	1.0	0.396	0.703	1.0	0.538	0.725	1.0

Table 5 AUROC score for Glow (Kingma & Dhariwal, 2018), likelihood ratio method (named ratio) (Ren et al., 2019), input complexity method (named IC) (Serrà et al., 2020) with a lossless PNG compressor, and all cases of the proposed method, namely the pure case (named P), including ratio (P+ratio) and including IC (P+IC). Models are trained on CelebA.

	$d = 3072$			$d = 1000$			$d = 500$		
	Glow	ratio	IC	P	P+ratio	P+IC	P	P+ratio	P+IC
Huber									
MNIST	0.0	0.001	1.0	0.0	1.0	1.0	0.0	1.0	1.0
FMNIST	0.13	0.004	1.0	0.014	0.906	1.0	0.017	0.906	1.0
Cifar10	0.7	0.624	0.655	0.703	0.276	0.442	0.707	0.276	0.442
LSUN	0.698	0.619	0.871	0.696	0.292	0.635	0.699	0.292	0.635
SVHN	0.061	0.	0.935	0.061	0.262	0.95	0.06	0.262	0.95
Constant	0.111	0.062	1.0	0.07	0.062	1.0	0.149	0.562	1.0
MSE									
MNIST	0.0	0.001	1.0	0.0	1.0	1.0	0.0	1.0	1.0
FMNIST	0.13	0.004	1.0	0.024	0.906	1.0	0.055	0.907	1.0
Cifar10	0.7	0.624	0.655	0.71	0.276	0.442	0.737	0.277	0.442
LSUN	0.698	0.619	0.871	0.707	0.293	0.635	0.738	0.293	0.635
SVHN	0.061	0.	0.935	0.062	0.262	0.95	0.059	0.261	0.95
Constant	0.111	0.062	1.0	0.077	0.565	1.0	0.187	0.572	1.0
	$d = 100$			$d = 50$			$d = 10$		
	P	P+ratio	P+IC	P	P+ratio	P+IC	P	P+ratio	P+IC
Huber									
MNIST	0.0	1.0	1.0	0.0	1.0	1.0	0.0	1.0	1.0
FMNIST	0.018	0.906	1.0	0.019	0.906	1.0	0.029	0.907	1.0
Cifar10	0.709	0.276	0.442	0.71	0.276	0.442	0.722	0.276	0.442
LSUN	0.699	0.292	0.635	0.696	0.292	0.635	0.703	0.292	0.635
SVHN	0.063	0.262	0.95	0.067	0.262	0.95	0.085	0.263	0.95
Constant	0.175	0.565	1.0	0.138	0.564	1.0	0.51	0.59	1.0
MSE									
MNIST	0.082	1.0	1.0	0.527	1.0	1.0	0.894	1.0	1.0
FMNIST	0.16	0.909	1.0	0.337	0.911	1.0	0.835	0.932	1.0
Cifar10	0.782	0.278	0.444	0.79	0.28	0.445	0.745	0.285	0.447
LSUN	0.785	0.295	0.637	0.801	0.297	0.639	0.75	0.301	0.641
SVHN	0.076	0.258	0.95	0.122	0.256	0.95	0.135	0.252	0.951
Constant	0.155	0.563	1.0	0.448	0.576	1.0	0.659	0.605	1.0

Fig. 5 The effect of changing the manifold dimension (d) and threshold value of the Huber loss (δ) on AUROC for trained models on SVHN.



6. Conclusion

NFs cannot directly provide an estimation of the likelihood on the data manifold. To address this, we adopted an algorithmic approach to jointly estimate the likelihood and data manifold, and used it for OOD detection. Our proposed method is based on the intuition that relying only on likelihood value on the manifold or reconstruction loss is insufficient for OOD detection. Accordingly, we found that using these two indicators, namely likelihood and reconstruction loss, jointly significantly improves OOD detection. Through extensive experiments, we showed the strength of the proposed method in finding data manifold and estimating its likelihood, besides showing excellent performance for image OOD detection. The proposed method can also generate samples similar to the latest state-of-the-art manifold learning using normalizing flows models in terms of visual quality. A per-pixel (or element-wise) Huber loss function was used in this paper for manifold learning. The Huber function was employed here due to its transition mode from linear to quadratic. It penalizes off-manifold parts linearly, and the model focuses on learning the on-manifold sub-space well. Per-object (a group of pixels) and per-sample (all pixels) loss can be an interesting work to follow in a future work. It should be noted that a primary assumption of the current study is that data lie on a manifold with one chart. In future work, we aim to extend a multi-chart version of the current method with possibly improved ability of OOD detection.

References

- Ardizzone, L., Mackowiak, R., Rother, C., & Köthe, U. (2020). Training normalizing flows with the information bottleneck for competitive generative classification. In *Advances in Neural Information Processing Systems* (pp. 7828–7840). Curran Associates, Inc. volume 33.
- Brehmer, J., & Cranmer, K. (2020). Flows for simultaneous manifold learning and density estimation. In *Advances in Neural Information Processing Systems* (pp. 442–453). Curran Associates, Inc. volume 33.
- Caterini, A. L., Loaiza-Ganem, G., Pleiss, G., & Cunningham, J. P. (2021). Rectangular flows for manifold learning. In *Advances in Neural Information Processing Systems* (pp. 30228–30241). Curran Associates, Inc. volume 34.
- Choi, H., Jang, E., & Alemi, A. A. (2019). Waic, but why? generative ensembles for robust anomaly detection. [arXiv:1810.01392](https://arxiv.org/abs/1810.01392).
- DeVries, T., & Taylor, G. W. (2018). Learning confidence for out-of-distribution detection in neural networks. [arXiv:1802.04865](https://arxiv.org/abs/1802.04865).
- Dinh, L., Sohl-Dickstein, J., & Bengio, S. (2017). Density estimation using Real NVP. In *International Conference on Learning Representations*. OpenReview.net.
- Goodfellow, I., Pouget-Abadie, J., Mirza, M., Xu, B., Warde-Farley, D., Ozair, S., Courville, A., & Bengio, Y. (2014). Generative adversarial nets. In *Advances in Neural Information Processing Systems*. Curran Associates, Inc. volume 27.
- Hendrycks, D., Mazeika, M., & Dietterich, T. G. (2019). Deep anomaly detection with outlier exposure. In *International Conference on Learning Representations*. OpenReview.net.
- Horvat, C., & Pfister, J.-P. (2021). Denoising normalizing flow. In *Advances in Neural Information Processing Systems* (pp. 9099–9111). Curran Associates, Inc. volume 34.
- Horvat, C., & Pfister, J.-P. (2022). Intrinsic dimensionality estimation using normalizing flows. In S. Koyejo, S. Mohamed, A. Agarwal, D. Belgrave, K. Cho, & A. Oh (Eds.), *Advances in Neural Information Processing Systems* (pp. 12225–12236). Curran Associates, Inc. volume 35.
- Huang, C.-W., Krueger, D., den Berg, R. V., Papamakarios, G., Cremer, C., Chen, R. T. Q., & Rezende, D. J. (2021). Normalizing flows across dimensions. In *International Conference on Machine Learning Workshop on Invertible Neural Networks, Normalizing Flows, and Explicit Likelihood Models*.
- Huber, P. J. (1964). Robust estimation of a location parameter. *The Annals of Mathematical Statistics*, 35, 73 – 101.

- Kalatzis, D., Ye, J. Z., Pouplin, A., Wohlert, J., & Hauberg, S. (2022). Density estimation on smooth manifolds with normalizing flows. [arXiv:2106.03500](https://arxiv.org/abs/2106.03500).
- Karras, T., Laine, S., Aittala, M., Hellsten, J., Lehtinen, J., & Aila, T. (2020). Analyzing and improving the image quality of stylegan. In *IEEE/CVF Conference on Computer Vision and Pattern Recognition* (pp. 8107–8116). Computer Vision Foundation / IEEE.
- Kim, H., Lee, H., Kang, W. H., Lee, J. Y., & Kim, N. S. (2020). SoftFlow: Probabilistic framework for normalizing flow on manifolds. In *Advances in Neural Information Processing Systems* (pp. 16388–16397). Curran Associates, Inc. volume 33.
- Kingma, D. P., & Ba, J. (2015). Adam: a method for stochastic optimization. In *International Conference on Learning Representations*.
- Kingma, D. P., & Dhariwal, P. (2018). Glow: Generative flow with invertible 1x1 convolutions. In *Advances in Neural Information Processing Systems*. Curran Associates, Inc. volume 31.
- Kingma, D. P., & Welling, M. (2014). Auto-encoding variational bayes. In *International Conference on Learning Representations*.
- Kirichenko, P., Izmailov, P., & Wilson, A. G. (2020). Why normalizing flows fail to detect out-of-distribution data. In *Advances in Neural Information Processing Systems* (pp. 20578–20589). Curran Associates, Inc. volume 33.
- Kothari, K., Khorashadizadeh, A., de Hoop, M. V., & Dokmanic, I. (2021). Trumpets: Injective flows for inference and inverse problems. In *Conference on Uncertainty in Artificial Intelligence* (pp. 1269–1278). AUAI Press volume 161 of *Proceedings of Machine Learning Research*.
- Krizhevsky, A., Nair, V., & Hinton, G. (2009). The CIFAR-10 dataset. <https://www.cs.toronto.edu/~kriz/cifar.html>.
- Kumar, N., Hanfeld, P., Hecht, M., Bussmann, M., Gumhold, S., & Hoffmann, N. (2021). Inflow: Robust outlier detection utilizing normalizing flows. [arXiv:2106.12894](https://arxiv.org/abs/2106.12894).
- LeCun, Y., & Cortes, C. (2010). The MNIST database of handwritten digits. <http://yann.lecun.com/exdb/mnist>.
- Lee, K., Lee, H., Lee, K., & Shin, J. (2018). Training confidence-calibrated classifiers for detecting out-of-distribution samples. In *International Conference on Learning Representations*. OpenReview.net.
- Liang, S., Li, Y., & Srikant, R. (2018). Enhancing the reliability of out-of-distribution image detection in neural networks. In *International Conference on Learning Representations*. OpenReview.net.

- Liu, Z., Luo, P., Wang, X., & Tang, X. (2015). Deep learning face attributes in the wild. In *IEEE International Conference on Computer Vision* (pp. 3730–3738). IEEE Computer Society.
- Murphy, K. P. (2022). *Probabilistic machine learning: an introduction*. MIT press.
- Nagarajan, V., Andreassen, A., & Neyshabur, B. (2021). Understanding the failure modes of out-of-distribution generalization. In *9th International Conference on Learning Representations*. OpenReview.net.
- Nalisnick, E. T., Matsukawa, A., Teh, Y. W., Görür, D., & Lakshminarayanan, B. (2019). Do deep generative models know what they don’t know? In *International Conference on Learning Representations*. OpenReview.net.
- Netzer, Y., Wang, T., Coates, A., Bissacco, A., Wu, B., & Ng, A. Y. (2011). Reading digits in natural images with unsupervised feature learning, .
- Pope, P., Zhu, C., Abdelkader, A., Goldblum, M., & Goldstein, T. (2021). The intrinsic dimension of images and its impact on learning. In *International Conference on Learning Representations*. OpenReview.net.
- Ren, J., Liu, P. J., Fertig, E., Snoek, J., Poplin, R., Depristo, M., Dillon, J., & Lakshminarayanan, B. (2019). Likelihood ratios for out-of-distribution detection. In *Advances in Neural Information Processing Systems*. Curran Associates, Inc. volume 32.
- Rezende, D. J., & Mohamed, S. (2015). Variational inference with normalizing flows. In *International Conference on Machine Learning* (pp. 1530–1538). JMLR.org volume 37 of *Workshop and Conference Proceedings*.
- Ross, B., & Cresswell, J. (2021). Tractable density estimation on learned manifolds with conformal embedding flows. In *Advances in Neural Information Processing Systems* (pp. 26635–26648). Curran Associates, Inc. volume 34.
- Serrà, J., Álvarez, D., Gómez, V., Slizovskaia, O., Núñez, J. F., & Luque, J. (2020). Input complexity and out-of-distribution detection with likelihood-based generative models. In *International Conference on Learning Representations*. OpenReview.net.
- Sohl-Dickstein, J., Weiss, E. A., Maheswaranathan, N., & Ganguli, S. (2015). Deep unsupervised learning using nonequilibrium thermodynamics. In *International Conference on Machine Learning* (pp. 2256–2265). JMLR.org volume 37 of *Workshop and Conference Proceedings*.
- Theis, L., van den Oord, A., & Bethge, M. (2016). A note on the evaluation of generative models. In *International Conference on Learning Representations*.
- Xiao, H., Rasul, K., & Vollgraf, R. (2017). Fashion-MNIST: a novel image dataset for benchmarking machine learning algorithms. [arXiv:1708.07747](https://arxiv.org/abs/1708.07747).

- Xiao, Z., Yan, Q., & Amit, Y. (2020). Likelihood regret: An out-of-distribution detection score for variational auto-encoder. In *Advances in Neural Information Processing Systems* (pp. 20685–20696). Curran Associates, Inc. volume 33.
- Yang, J., Zhou, K., Li, Y., & Liu, Z. (2022). Generalized out-of-distribution detection: A survey. [arXiv:2110.11334](https://arxiv.org/abs/2110.11334).
- Yu, F., Seff, A., Zhang, Y., Song, S., Funkhouser, T., & Xiao, J. (2016). Lsun: Construction of a large-scale image dataset using deep learning with humans in the loop. [arXiv:1506.03365](https://arxiv.org/abs/1506.03365).
- Zhang, L. H., Goldstein, M., & Ranganath, R. (2021). Understanding failures in out-of-distribution detection with deep generative models. In *International Conference on Machine Learning* (pp. 12427–12436). PMLR volume 139 of *Proceedings of Machine Learning Research*.
- Zisselman, E., & Tamar, A. (2020). Deep residual flow for out of distribution detection. In *IEEE/CVF Conference on Computer Vision and Pattern Recognition* (pp. 13991–14000). Computer Vision Foundation / IEEE.